

# Petrophysical characterization and formation evaluation of sandstone reservoir: Case study from Shahd field, Western Desert, Egypt

Basem CHIKIBAN\* , Moustafa H. KAMEL , Walid M. MABROUK ,  
Ahmed METWALLY 

Geophysics Department, Faculty of Science, Cairo University, Giza, Egypt

**Abstract:** This paper aims to establish a complete workflow for a petrophysical evaluation to enhance and quantify hydrocarbon prospect and productivity of Shahd SE field, East Ras Qattara concession, Western desert, Egypt. The suggested workflow can, then, be used with the same steps and sequences for any petrophysical evaluation study. Well logs data from four wells were used for this study. The present data has drilled through three formations: (1) Bahariya Formation, which has been divided into two sub-zones; (I) Upper Bahariya, a shaly formation and (II) Lower Bahariya, the main reservoir present in our case study. (2) Kharita Formation, which consist of clean sand. We will evaluate the three most useful petrophysical parameters: (a) volume of shale ( $V_{sh}$ ) using the gamma-ray (GR), (b) effective porosity ( $\phi_{eff}$ ) using the neutron log and the resulting volume of shale as an input, and (c) water saturation ( $S_w$ ). Several equations were used to calculate the  $S_w$ . The best equation was Simandoux equation to put in consideration the shale model of the upper Bahariya. The results show that the net reservoir and net pay thicknesses were seen very promising in all four wells, all at the lower Bahariya Formation. The reservoir quality parameters “Effective Porosity ( $\phi_{eff}$ )” were almost the same for all four wells, as well as the high hydrocarbon saturation “Sh” for all four wells.

**Key words:** Shahd SE field, formation evaluation, litho-saturation model, petrophysical interpretation workflow

## 1. Introduction

The reservoir studies through petrophysical evaluation can be achieved in three steps: (1) Log quality control (LQC); this step varies from a user to another. Its main purpose is to correct all expected errors and issues in the log data recording to give a better log data display and better results (*Bassiouni, 2012*). (2) Qualitative interpretation; consisting of a full log display including gamma ray (GR), resistivity (deep, transition and

\*corresp. author, e-mails: basemhosny@gstd.sci.cu.edu.eg; basem.chikiban@gmail.com

shallow), density (RhoB), neutron (NPhi) and photoelectric (PE). Its purpose is to establish a general overview and expectation of the subsurface formation properties. Alongside the log display, we will use a lithology (NPhi-RhoB) cross-plot to confirm the type of matrix. (3) Quantitative interpretation; we will start by studying each well with a Picket plot. Pickett's plots (resistivity-porosity cross-plots) are powerful in obtaining more information than any other petrophysical technique. They have been recognized as very useful approach in petrophysical interpretation.

Then, we will build a Litho-saturation model using the following petrophysical parameters: (a) volume of shale (Vsh), (b) effective porosity ( $\phi_{eff}$ ) and (c) water saturation (Sw). The litho-saturation model helps giving an overview of the well potentiality.

## 2. Geological settings

Shahd field is in the East Ras Qattara concession, Western desert, Egypt, at about 200 kilometers from Cairo, in Matrouh governorate, Western desert (Fig. 1). The main reservoir rock in this area is the Bahariya Formation, a

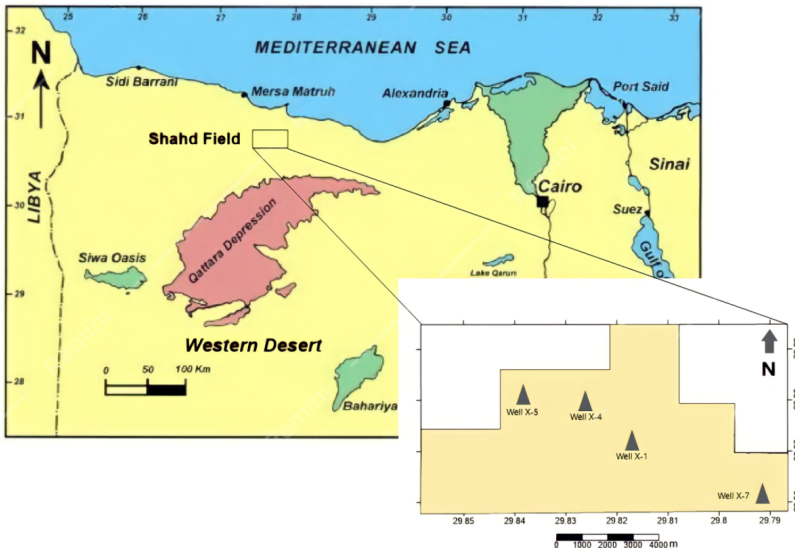


Fig. 1. Location and base map of Shahd Field, East Ras Qattara concession, Western desert, Egypt. Modified after *Kassab et al. (2017)*.

mixed Clastic and carbonate deposited during both late Albian and early Cenomanian age under a tidal environment. The Shahd SE field is known to have a complex and challenging geological setting. According to (*Abu El-Ata, 1990*) and (*Mostafa et al., 2018*), it has a NW–SE trending faults from the Cretaceous age forming one of the most leading and well-known horst structure in the western desert of Egypt.

This structure is, in fact, affecting the Bahariya Formation, the main productive zone of the East Ras Qattara concession. Bahariya Formation is a main oil reservoir in the North Western Desert of Egypt (*Mostafa et al., 2018*). The main trend of the fault structure is from the late Cretaceous era initiated by a dextral shear tectonic movement which occurred during that time (*Abu El-Ata, 1990*). Due to this complex geology, the Bahariya Formation displays a tidal channel geometry that varies vertically and laterally. The lithological composition, sedimentary structure and bioturbations studies also indicate that the Bahariya deposition was in tidal flat facies and lagoon.

Figure 2 shows a general lithostratigraphic column of the north Western Desert. The basin of Ras Qattara has potential hydrocarbon traps within the Upper Cretaceous (late Albian) sandstone of the Bahariya Formation, also known as the lower Bahariya Formation. The upper Bahariya deposition was during the early Cenomanian (*Temraz et al., 2009*). It consists mostly of shale and is considered a potential source rock.

### 3. Available data

The available data were digitized from consulted master thesis (*Soliman, 2021*). The well reports are concealed due to confidentiality reasons. Operations at the given fields are still in progress. The data consists of four wells, each well contain: Gamma-ray (GR) log, Neutron ( $\phi N$ ) log, Density ( $\rho b$ ) logs, resistivity (Res Deep, MSFL, Res Shall) logs and photoelectric (PE) log. Along with them comes a detailed formation tops for each well.

### 4. Methodology

Figure 3 represent the petrophysical interpretation workflow that will be applied for this case study. The software programs used are Techlog for

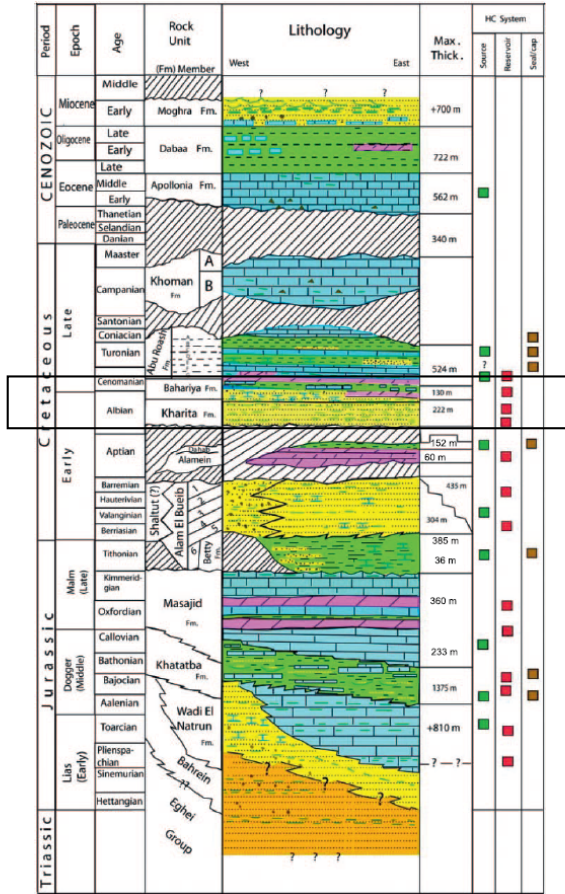


Fig. 2. Generalised stratigraphic column of the North Western Desert, Egypt with main elements of the petroleum system. Modified after *Moretti et al. (2010)*.

petrophysical analysis, Surfer for mapping and Neuralog for well data digitization.

**I. Data preparation and Log quality control (LQC)**

For better log data display and results, we start with a log quality control (LQC). We applied several steps of log quality control which consist of:

1. As a first step of data preparation, we do a simple step known as “(1) digitization and redrawing” where we draw the digitized data and match

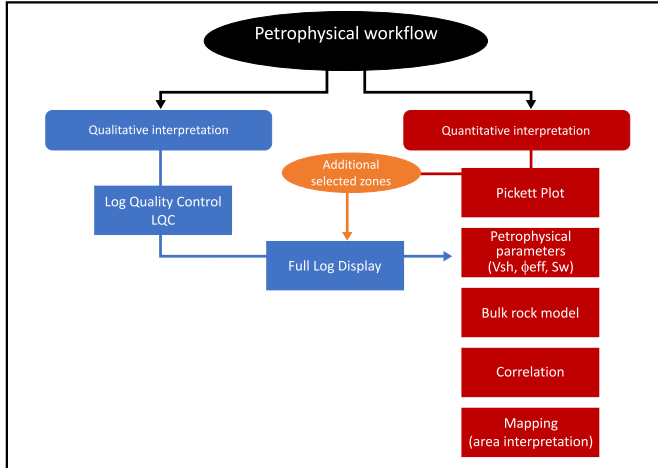


Fig. 3. Petrophysical analysis and well logs interpretation workflow.

it with the raw data. This is to insure whether the sampling interval is correct or not.

2. The second step is “(2) depth matching”, a very efficient step to avoid any kind of depth shifting error. It is done due to the different measurement techniques for each tool. As we know, some tools record continuously and others records stationary. Therefore, a shift may occur in the logged data and must be corrected by using one specific tool as a reference (*Hassan et al., 2014*). We usually take the gamma-ray (GR) log response as our reference for the depth matching to the other logs.
3. For a better log display conception, it is recommended to rescale the logged data to the known standard scales. Also, we should “clean up” the logged data from all pikes due to bad record. This step is known as “(3) rescaling”.
4. Our next step in data preparation is identifying both “(4) washout and mud cake”. They can be determined using both calibre tool and the bit size. Both are good indicator of the formation condition especially in term of permeability.
5. Finally, for our analysis and calculations, we will require as inputs some of the “(5) shale parameters” for each formation: shale density, shale porosity, shale (maximum) gamma-ray and shale resistivity ( $\rho_{sh}$ ,  $\phi_{sh}$ ,

GRsh, and Rsh). These values can be picked from the logged data as the corresponding values beside the highest gamma ray zone for each formation.

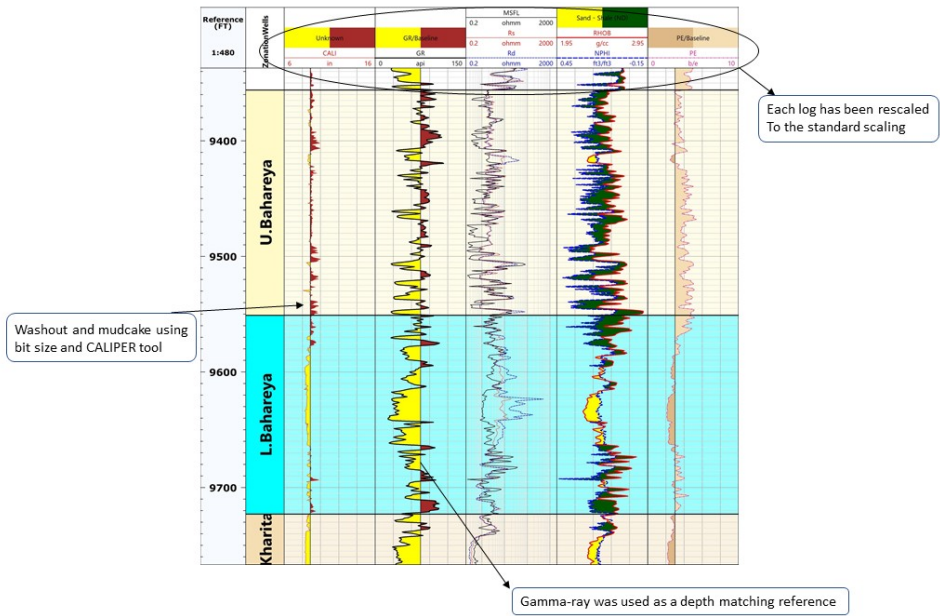


Fig. 4. Data log display after log quality control (LQC).

## II. Log display and matrix identification

Our log display is illustrated as shown in Fig. 4. Our objective from the log display is to identify the potential zones (1) and the matrix type (2).

### 1. Potential zones

In this step, we make a quick overview of our data and choose the zones that have certain criteria. The most important criteria are a high deep resistivity with or without gap of the shallow resistivity and deep resistivity. This gap indicates that the zone was flushed away, and the formation mostly contain hydrocarbon. Alongside the high deep resistivity, we check if the zone has a low gamma ray, crossover display of the RhoB-PhiN log. If the zone matches all those criteria, it is highlighted to be studied furthermore using Pickett plot (Fig. 5).

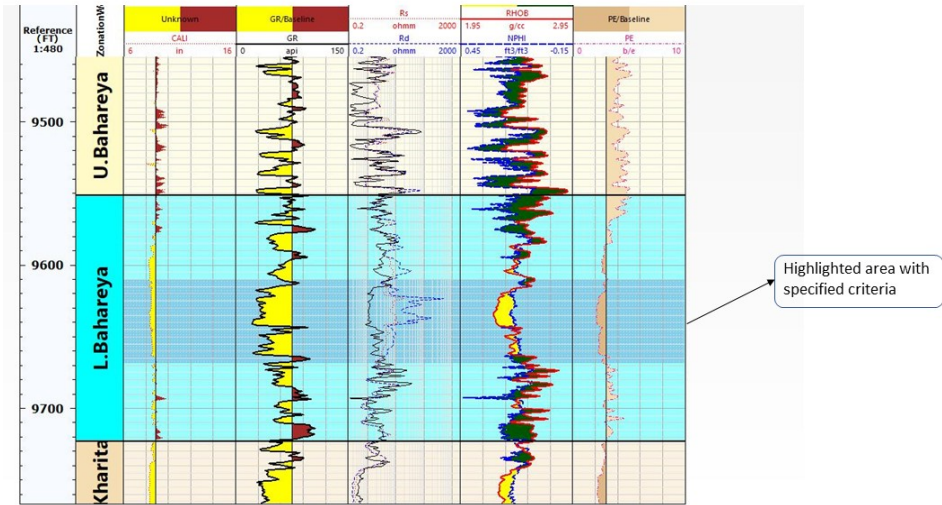


Fig. 5. Highlighted zone of interest.

## 2. Matrix identification

With our present data, the best way to study the lithology will be using a lithology cross-plot between density log (RhoB) and neutron log (PhiN). This cross-plot helps identifying the lithology of oil or water-filled formations that are pure lithology of limestone, sandstone, or dolomite. Yet, when it comes to mixed mineralogy, like calcareous-cemented sandstone, the density-neutron cross-plot analysis can be enigmatic. Hence, for better result, we will also correlate the results of the cross-plots with the photoelectric log (PE).

In a case where there is some clay in the sandstone, the cross-plot will go toward the shale zone. If we add some gas to that same sandstone, the cross-plot will interpret it as clean sandstone. Another case is when gas is present in dolomite. It will be present in the clean limestone zone of the cross-plot. These cases show us why it is critical to know in advance of the stratigraphic details (*Alberty, 1994*).

The correlation between the photoelectric log (PE) and the MID plot (RhoB-PhiN cross-plot) appear to be very effective in our lithology identification. In well X4, we found a small, laminated bed of limestone in the middle of a shaly sand zone (Fig. 6). Upon using the MID plot, the given

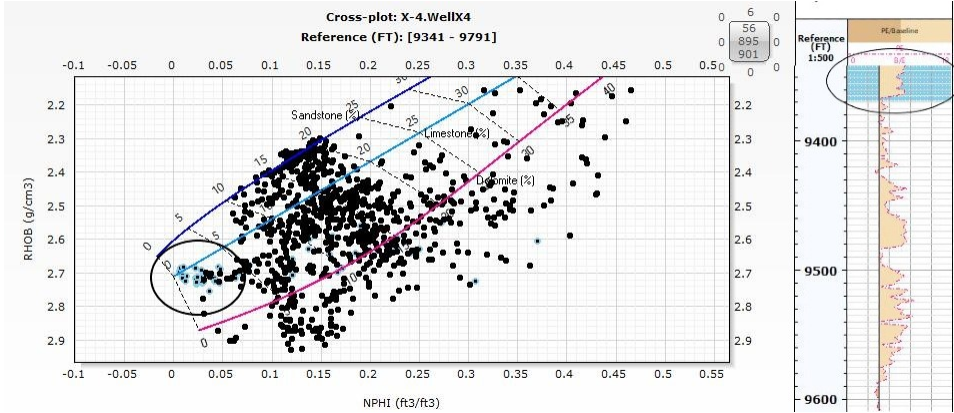


Fig. 6. Correlation of a) MID plot with b) PE log for matrix identification of well X4. The black circle in the PE log was interpreted as limestone. The black circle in the MID cross-plot is the corresponding zone of the PE log.

response was, indeed, of limestone. Since some anomalies can be found in the MID plot due to the mixed lithology, we confirmed the identity of this zone by using the PE log response. The response of the photoelectric log gave the same interpretation, which is limestone.

Another effective way to study the accuracy of the MID plot is to introduce a colour coding in the cross-plot. In this case (Fig. 7), adding the gamma-ray (GR) respond as a colour coding will insure if the cross-plot

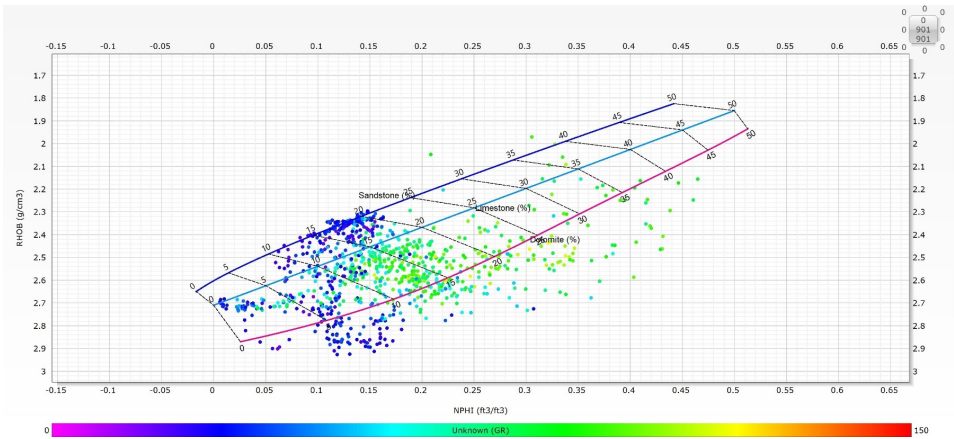


Fig. 7. MID plot for Well X4 with gamma-ray log added as colour coding.

interpretation is coherent or not. For example, we should expect a low gamma-ray response at the sandstone zone of the MID chart. Otherwise, there might be an anomaly and further studies are required.

### III. Rw determination and productive zone selection (Pickett Plot)

Named after *Pickett (1973)*, the main idea behind Pickett plot is to establish an effective technique to solve Archie's equation without the need of constants. This approach is based on cross-plot between the formation resistivity (Rw) and the neutron porosity ( $\phi_N$ ) with a pattern recognition. One of the many benefits is that water saturation can be predicted without calibrating any data for the porosity measuring device (like density ( $\rho_b$ )). Another benefit is that you don't need to know the water resistivity, and even better, you can derive its value from the cross-plot. It is very important to plot data of a significant number of zones to provide accurate calculation (*Shazly, 2009*).

Archie's equation, the formation factor (F), porosity ( $\phi_N$ ), water saturation (Sw), and resistivities Rw, in granular rocks states that:

$$F = \frac{R_o}{R_w} = \frac{a}{\phi^m}, \quad (1)$$

$$S_w^n = \frac{R_o}{R_t}, \quad (2)$$

where:

$a$  = proportionality constant (from 0.6 to 1.5);

$m$  = cementation factor (from 1.2 to 2.9);

$n$  = saturation exponent, often assumed to be 2;

$R_o$  = resistivity of the formation at 100% Sw;

$R_w$  = resistivity of the formation water;

$R_t$  = true resistivity of the formation.

Hence, from both Eqs. (1) and (2), we have that:

$$m \log(\phi) = \log a R_w - \log R_t - n \log S_w. \quad (3)$$

Figure 8 shows the Pickett plot for well X1, we derived the Rw value at the extension of the slope at porosity 100% and the highlighted additional selected productive zone. We highlighted additional zone at the slope of water saturation Sw = 50%.

Our cut-off for the Sw is 50%. Any zone above this range is considered a potential oil bearer zone and should be studied in detail. Figure 9 is the corresponding log display of the additional selected productive zone.

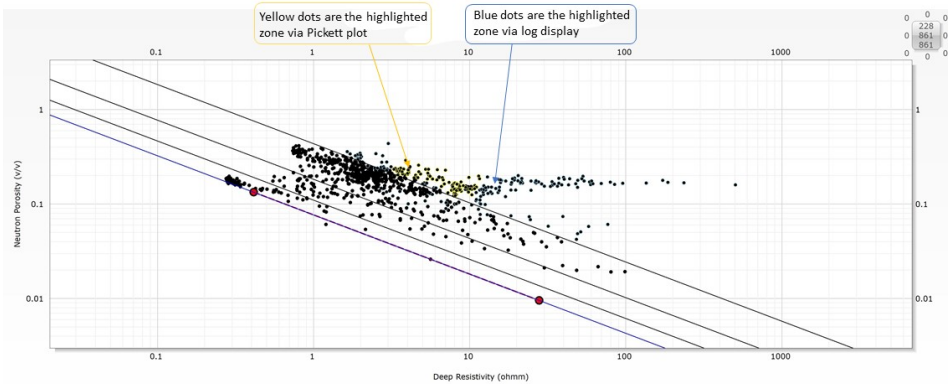


Fig. 8. Pickett plot of well X1, the yellow dots are the additional highlighted productive zones.

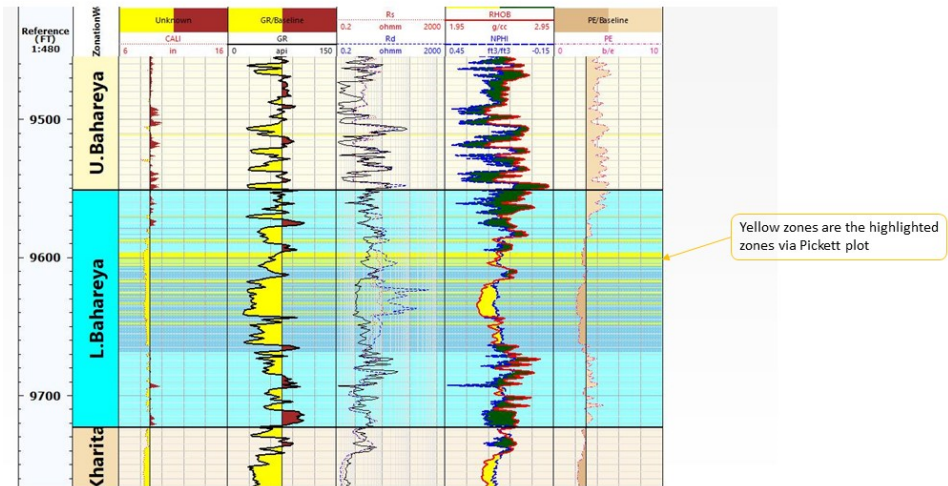


Fig. 9. Log display of the corresponding yellow zones of Pickett plot. The yellow zones are the additional zones selected via Pickett plot.

#### IV. Petrophysical parameters calculation

There are mainly three important petrophysical parameters that must be calculated: Volume of shale (1), effective porosity (2), water saturation (3).

These parameters should be calculated in this same order since they are dependent on each other.

### 1. Shale volume determination

It is the first and most critical parameter to calculate. This is because as we mentioned before, all other petrophysical parameters (effective porosity and water saturation) will be dependent on the volume of shale (Vsh). The volume of shale has a great impact in log interpretation. In a porous-permeable formation, if the volume of shale is under-estimated, the calculation of the effective porosity will be optimistic, while if the volume of shale over-estimated, the calculation of the effective porosity will be pessimistic (*Kamel and Mabrouk, 2003*). Therefore, the volume of shale must be calculated precisely.

One of the most used equations for shale volume calculation, and the one we applied in our case study, is the linear gamma-ray index equation:

$$V_{sh} = \frac{GR_{Log} - GR_{min}}{GR_{max} - GR_{min}}. \quad (4)$$

However, quite often the resulting Vsh yields an over-estimated volume of shale, producing a pessimistic interpretation of the reservoir quality. Therefore, the final value should be corrected using one of the methods introduced by *Clavier et al. (1971)* or *Steiber (1973)*. In our case, we used Steiber equation for volume of shale correction:

$$V_{shSteiber} = \frac{0.5 * V_{sh}}{1.5 - V_{sh}}, \quad (5)$$

$$V_{shClavier} = 1.7 - \sqrt{3.38 - (V_{sh} + 0.7)^2}, \quad (6)$$

$$V_{shLarionov \text{ old rock}} = 0.33 (2^{2(V_{sh})} - 1), \quad (7)$$

$$V_{shLarionov \text{ tertiary rock}} = 0.083 (2^{3.7(V_{sh})} - 1), \quad (8)$$

where:

Vsh = volume of shale;

GR<sub>Log</sub> = gamma ray reading;

GR<sub>max</sub> = maximum gamma ray (shale);

GR<sub>min</sub> = minimum gamma ray (clean sand or carbonate).

## 2. Effective porosity calculation

To derive the precise value of the water saturation ( $S_w$ ) and other parameters like the formation factor ( $F$ ), permeability ( $k$ ) and bulk volume of water (BVW), we need to determine the value of the effective porosity (*Abuzaied et al., 2020*). It's the portion of the total porosity that is interconnected allowing fluids to move through it.

$$\phi_{\text{eff}} = \phi N - (V_{\text{shSteiber}} * \phi_{\text{sh}}) . \quad (9)$$

Another method to calculate the effective porosity by using the density tool is:

$$\phi_{\text{eff}} = \phi D - (A * V_{\text{sh}}[\text{dec}]) , \quad (10)$$

where:

$$\phi D = \frac{\rho_m - \rho_b}{\rho_m - \rho_{\text{fl}}} , \quad (11)$$

$$A = \frac{\rho_m - \rho_{\text{sh}}}{\rho_m - \rho_{\text{fl}}} , \quad (12)$$

where:

$\phi_{\text{eff}}$  = effective porosity;

$\phi N$  = neutron porosity or total porosity;

$\phi_{\text{sh}}$  = shale porosity;

$V_{\text{shSteiber}}$  = corrected volume of shale;

$\rho_m$  = density of matrix, standard value ( $\rho_{\text{ma}} = 2.68 \text{ g/cm}^{-3}$ );

$\rho_b$  = density log value;

$\rho_{\text{fl}}$  = density of pore fluids, standard value ( $\rho_{\text{f}} = 1.0 \text{ g/cm}^{-3}$ );

$\rho_{\text{sh}}$  = density of shale, from laboratories measurement ( $\rho_{\text{sh}} = 2.42 \text{ g/cm}^{-3}$ );

$V_{\text{sh}}$  = volume of shale, in decimal;

$A$  = shale correction.

## 3. Fluid saturation calculation

It is important to put in consideration that the fluid saturation calculation method varies from a clean formation to a shaly formation.

- Clean formation:

A clean formation is considered a formation with homogenous intergranular porosity. There are several methods to calculate the fluid saturation

of a clean formation, one of them is considered the most common and widely used equation, Archie's equation (*Archie, 1942*).

$$S_w^n = \frac{F \cdot R_w}{R_t}, \quad (13)$$

$$F = \frac{a}{\text{PHI}_E^m}, \quad (14)$$

where:

$S_w$  = water saturation of the uninvaded zone;

$n$  = saturation exponent (usually equal 2);

$R_w$  = formation water resistivity;

$F$  = formation factor;

$R_t$  = formation resistivity (real measured resistivity);

$a$  = a factor dependent on lithology ( $a = 1$ );

$m$  = cement factor ( $m = 2$ );

$\text{PHI}_E$  = porosity (effective porosity).

A similar equation with the same expression has been established for the flushed zone saturation.

$$S_{xo}^n = \frac{F \cdot R_{mf}}{R_{xo}}, \quad (15)$$

where:

$S_{xo}$  = water saturation of the invaded zone;

$R_{xo}$  = resistivity of the invaded zone.

Other methods exist like the Resistivity Ratio Method. It determines the clean formation water saturation by assuming that the formation itself is divided to two zones: the flushed zone and uninvaded zone. Both zones have the same formation resistivity factor ( $F$ ), but different water resistivity ( $R_w$  &  $R_{mf}$ ).

$$\left( \frac{S_w}{S_{xo}} \right)^2 = \frac{R_{xo}/R_t}{R_{mf}/R_w}. \quad (16)$$

In this equation, the saturation exponent ( $n$ ) is assumed to be 2. Also, the knowledge of formation factor or porosity is not required. For this method to be applied, the resistivity of the two assumed zones must be measured from log or calculated. Also, methods for determining the wa-

ter resistivity of both zones must be available. This method is useful when no porosity or formation factor data are available, but because of the necessary assumptions, the resistivity ratio methods have limitations. The main limitation came from the inability of any resistivity measurement tool to measure either  $R_{xo}$  or  $R_t$  independently. But now,  $R_{xo}$  can be measured independently using the micro-spherical focused tool (MSFL). Another limitation appears when hydrocarbon is present in the formation. In that case, knowledge or even assumption of the invaded zone saturation ( $S_{xo}$ ) is required.

- Shaly formation:

Identifying shales or even shaly formations are essential in log analysis. Not only do they affect porosity calculations as we mentioned before, but do to their electrical properties, they have a great influence on the determination of fluid saturation. In this matter, *Archie (1942)* proposed a modified form for his equation putting in consideration shale's parameters.

$$S_w = \sqrt{F \cdot R_w * \left( \frac{1}{R_t} - \frac{V_{sh}}{R_{sh}} \right)}. \quad (17)$$

*De Witte (1950)* developed another model for dispersed clay type in a clean sand formation. The dispersed clay equation takes the quadratic form equation:  $Ax^2 + bx + c = 0$  (11). Hence, the equation took the following form:

$$S_w = \frac{R_w}{2\phi} \left[ -y + \sqrt{y^2 - \left( \frac{4}{R_w} \right) * \left( \frac{V_{sh}^2}{R_c} - \frac{1}{R_t} \right)} \right]. \quad (18)$$

His results showed that the value of water saturation will be too low in low resistivity pay sand. But in case shaly sand, the water saturation values will be more credible.

*Poupon et al. (1954)* developed a model for shaly sand interpretation consisting of two media present in alternate layers. Therefore, the following equation is valid for water saturation calculation in both clean and shaly sand.

$$S_w = \sqrt{\frac{a}{\phi^m} \left[ \frac{1}{R_t} - \frac{V_{sh}}{R_{sh}} \right] \frac{R_w}{(1 - V_{sh})}}. \quad (19)$$

*Simandoux (1963)* developed one of the most efficient water saturation equations known as the total shale equation. This equation was supported by experiments at the French Institute of Petroleum:

$$S_w = \left[ \left( \frac{-V_{sh}}{R_{sh}} \right) + \sqrt{\left( \frac{-V_{sh}}{R_{sh}} + \frac{5\phi^2}{R_t R_w} \right)} \right] \frac{0.4 R_w}{\phi^2}. \quad (20)$$

Another model was established by Poupon and Leveaux in 1971 (*Poupon and Leveaux, 1971*) where it showed that the calculated water saturation is a function depending on the rate of shale of the reservoir and the true resistivity. This model was called Indonesian model:

$$S_w = \left[ \frac{V_{sh}^{0.5(1-V_{sh})}}{\left( \frac{R_{sh}}{R_t} \right)^{0.5} + \left( \frac{R_{sh}}{R_o} \right)^{0.5}} \right]^{-2/n}. \quad (21)$$

*Kamel (1993)* elaborated an innovative equation for water saturation calculation that is practically valid for many shaly formations. His equation focused on the benefits and validity of calculating the clean formation resistivity ( $R_o$ ), which showed a good agreement with Simandoux and Indonesian equation:

$$S_w = \sqrt{\left( \frac{R_o}{R_t} + \left[ \left( \frac{R_o}{R_{sh}} \right) (2V_{sh}) \right]^2 \right)} - \sqrt{\left[ \left( \frac{R_o}{R_{sh}} \right) (2V_{sh}) \right]^2}. \quad (22)$$

Another brilliant approach was made by *Kamel et al. (1996)* where he adjusted the Schlumberger equation by adding the cementation exponent ( $m$ ) and cementation factor ( $a$ ):

$$S_w = \frac{\left[ \left( \frac{-V_{sh}}{R_t} \right) + \sqrt{\left( \frac{-V_{sh}^2}{R_{sh}^2} + \frac{\phi_T^2}{0.2 R_t R_w (1 - V_{sh})} \right)} \right]}{\frac{\phi_T^2}{0.4 R_t R_w (1 - V_{sh})}}. \quad (23)$$

Since both are related to the formation factor (F), it will give as a result a computed water saturation value within a range of 5%.

$$S_w = \frac{\left[ (V_{sh} \cdot R_t) + \sqrt{\left( V_{sh}^2 \cdot R_t^2 + \frac{4 R_t \cdot R_{sh}^2}{F R_w (1 - V_{sh})^2} \right)} \right]}{\frac{2 R_t R_{sh}}{F R_w (1 - V_{sh})^2}}. \quad (24)$$

For our researched we used Simandoux model (*Simandoux, 1963*) for water saturation. Then we used the product of the computed water saturation water ( $S_w$ ) and its corresponding porosity to calculate the bulk volume of water (BVW). The bulk volume of water will be used in the final quantitative interpretation step: the bulk rock model:

$$BVW = S_w * \phi, \quad (25)$$

where:

BVW = bulk volume water;

$S_w$  = computed water saturation of uninvasion zone;

$\phi$  = porosity (total).

#### 4. Total bulk volume of fluids and effective porosity

To confirm the accuracy of the effective porosity, we can compare it with the total bulk volume of fluids. The total bulk volume of fluid is the sum of all fluids present in the invaded formation:

$$\phi_{\text{eff}} = BVW + BVHR + BVHM, \quad (26)$$

$$BVHR = BVHC - BVHCM, \quad (27)$$

where:

BVW = bulk volume water;

BVHC = bulk volume of hydrocarbon;

BVHM = bulk volume of movable hydrocarbon;

BVHR = bulk volume of residual hydrocarbon.

The percentage of error in our case study was 0% (Fig. 10).

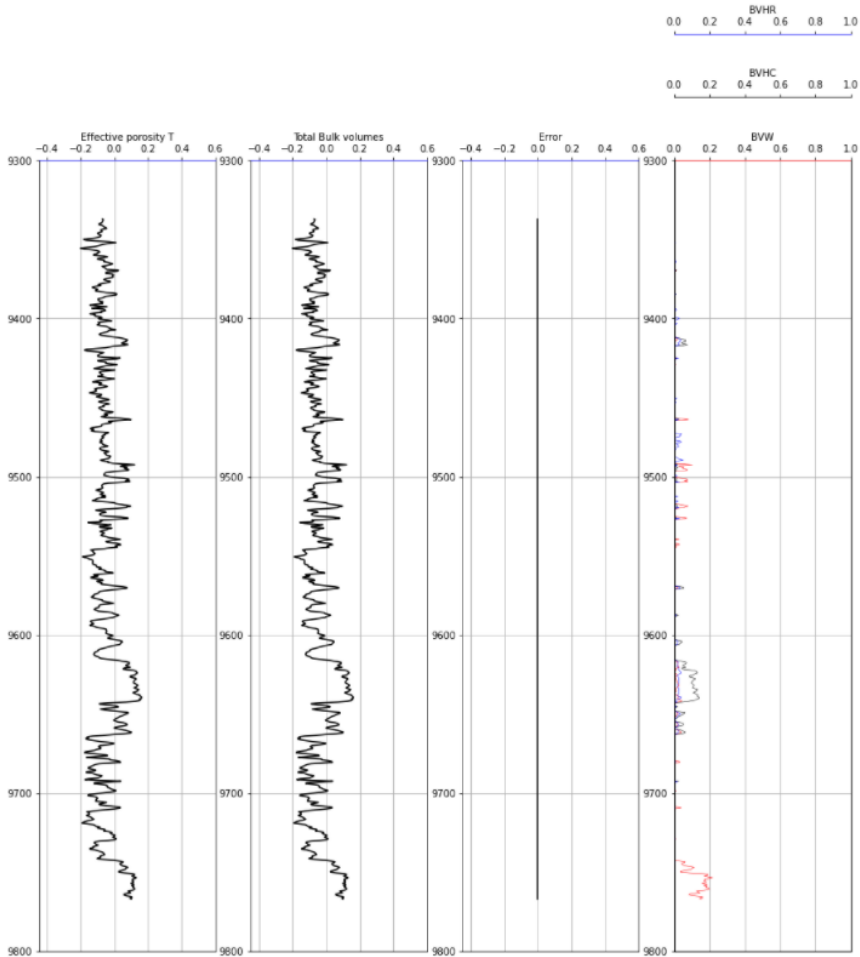


Fig. 10. Comparison between effective porosity and total bulk volume.

### 5. Well correlation and mapping interpretation of the area

For a better understanding of our reservoir capacity, correlating the four bulk rock volume of the five present wells can be handy (Fig. 11) and can also give a full view of the reservoir extension (vertically and laterally).

From the Vsh contour map (Fig. 12), the volume of shale in lower Bahariya Formation decreases to the south east direction. A clear moderate dipping of the volume of shale can be seen toward the east.

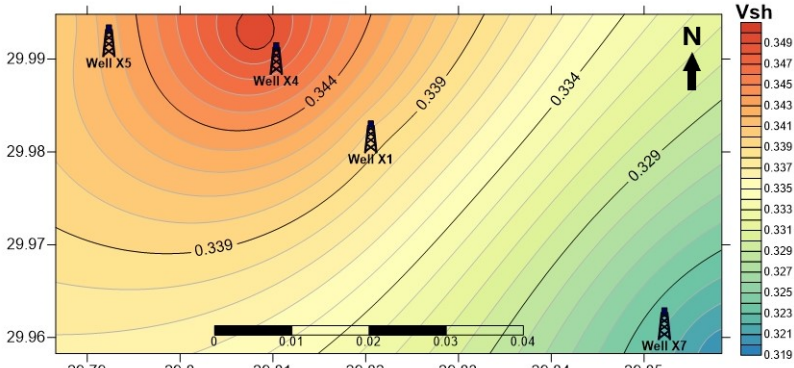


Fig. 11. Volume of shale (Vsh) Contour map of lower Bahariya.

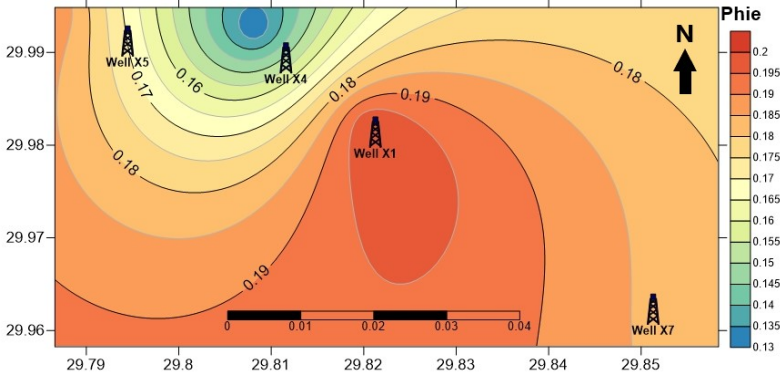


Fig. 12. Effective porosity (Phie) contour map of lower Bahariya.

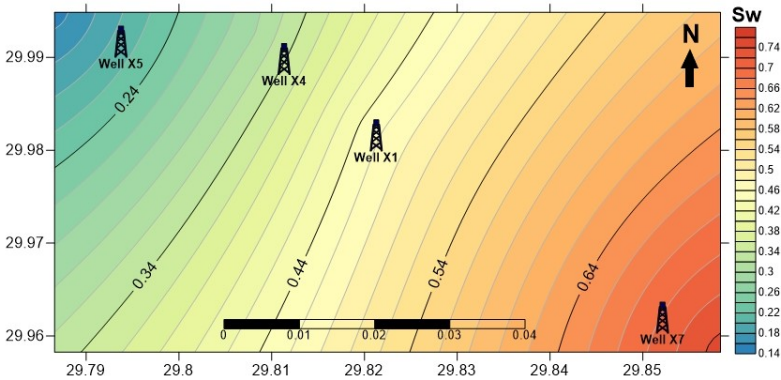


Fig. 13. Water saturation (Sw) contour map of lower Bahariya.

The Phie contour map (Fig. 13) indicates a decrease in the effective porosity in lower Bahariya Formation toward the north-west. Precisely, a steep dipping of the Phie is clear toward the north between Well X5 and X4 location.

## 6. The bulk rock model

It is the final model used for petrophysical interpretation. Displayed as a log, it describes what the formation is divided into as shown in Fig. 14. The bulk rock volume is composed of the three calculated petrophysical parameters: volume of shale, effective porosity, and bulk volume of water. The model will clarify the percentage of matrix volume alongside the volume of shale and the percentage of hydrocarbon saturation. The volume of matrix can be divided into matrix constituent like limestone, sandstone, anhydrite,... etc. As an equation, the bulk rock model can be expressed as following:

$$V_{sh} + V_{matrix} + \phi_{eff} = 1, \quad (28)$$

where  $\phi_{eff} = BVW + BVHC + BVHM$ .

As for the water saturation in lower Bahariya Formation, the  $S_w$  contour map (Fig. 14) shows a monotonic increase toward the east, making the lower Bahariya Formation at Well X5 the highest reservoir containing oil as the hydrocarbon saturation decreases laterally all the way to Well X7.

## 5. Results

The outcome of the petrophysical evaluation showed that this concession has a very promising hydrocarbon reservoir. Each well showed that the lower Bahariya Formation contains a promising net pay reservoir. Only well-X7 showed that the hydrocarbon is present in upper Bahariya Formation.

The highest net pay zone is 200 ft. at the lower Bahariya of well-X5, while the lowest is 35 ft. at the upper Bahariya of well-X7 (Fig. 15). The highest hydrocarbon saturation is 90% at the lower Bahariya of well-X5, while the lowest hydrocarbon saturation is 65% at the upper Bahariya of well-X7. This shows that Well-X5 is the most promising well for production.

In well-X7, Kharita Formation showed low hydrocarbon saturation while in the three other wells it showed the 100% water saturation (no hydrocarbon saturation). It's important to mention that while Kharita Formation

Table 1. Petrophysical parameter values for each well.

	Gross Thickness (ft)	Net Reservoir (ft) Cutoff: < 30 ft	Net pay (ft) Cutoff: < 15 ft	PhiE (%) Cutoff: < 10%	Vsh (%) Cutoff: > 50%	Sw (%) Cutoff: > 70%
U. Bahariya X1	195	15	8	15	38	80
L. Bahariya X1	172	70	50	16	34	30
Kharita X1	N/A	0	0	15	31	100
U. Bahariya X4	187	4	0	13	38	85
L. Bahariya X4	239	117.5	65	13	35	30
Kharita X4	N/A	0	0	16	4	100
U. Bahariya X5	191	8	0	13	33	70
L. Bahariya X5	267	210	200	13	34	10
Kharita X5	N/A	0	0	18	10	100
U. Bahariya X7	126	41	35	14	32	40
L. Bahariya X7	161	13	8	13	34	35
Kharita X7	N/A	0	0	17	27	100

starts at depth 9750 ft in well-X1, well-X4 and well-X5, Kharita Formation starts from depth 10000 ft at well-X7. We suggest further studies on Kharita Formation at the southwest direction of well-X7.

## 6. Conclusion

This paper displays a full petrophysical evaluation aiming to improve the reservoir production of Shahd field. From the interpretation, the following conclusion has been reached:

The main reservoir in Shahd field is Bahariya Formation, both upper and lower. From the lithology cross-plot, it consists mainly of sandstone mixed with few limestones. The average total porosity is 19%, and the average effective porosity is 13%, indicating a good reservoir quality (Table 1).

From the hydrocarbon indicators and petrophysical parameters calculation, the hydrocarbon is present from Well X5, X4 and X1 in lower Bahariya Formation, while Well X7 has hydrocarbon in upper Bahariya. This might be due to a structural feature event (maybe normal fault) causing the oil to be trapped in upper Bahariya.

The net pay reservoir is decreasing throughout the four wells starting from the west, Well X5, which has the highest net pay reservoir, to the east, Well X7, which has the lowest net pay reservoir.

Kharita Formation showed some traces of hydrocarbon saturation at well-X7 while the three other wells didn't show any sign of hydrocarbon.

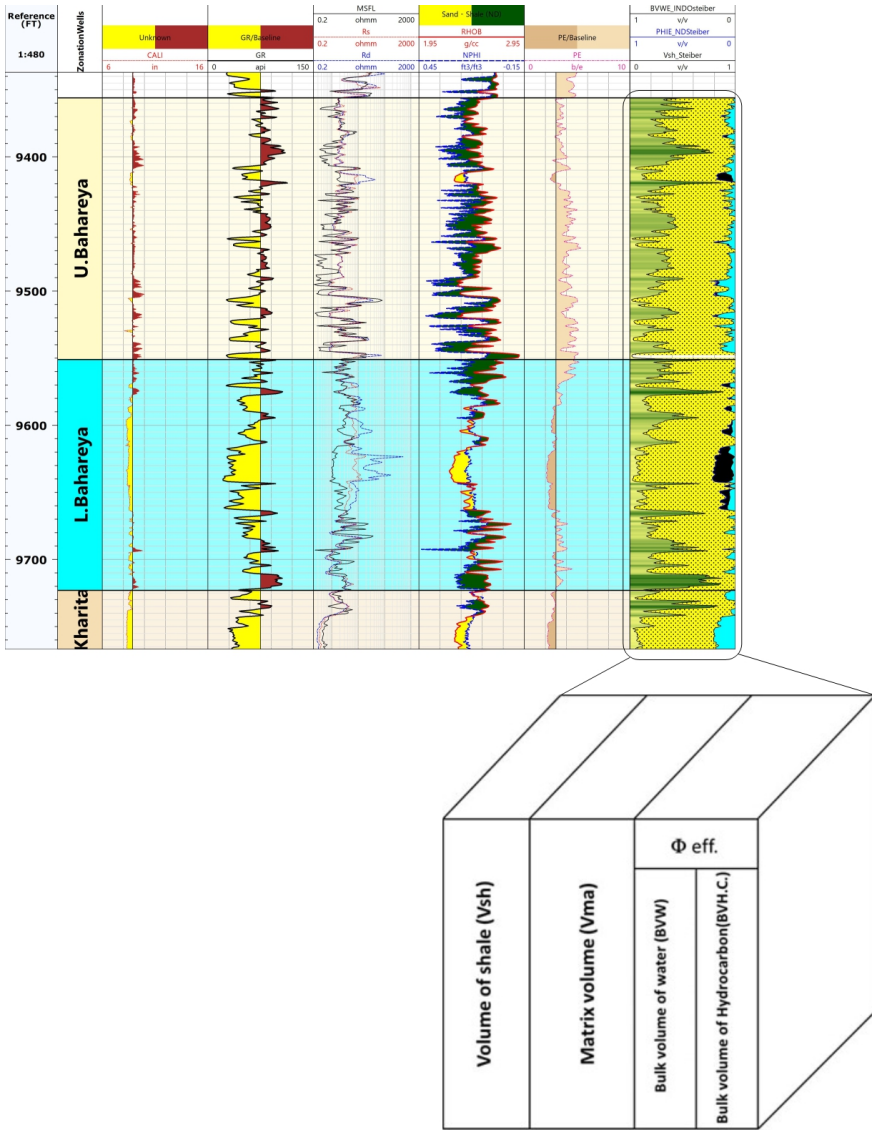


Fig. 14. The formation rock (litho-saturation model) model of well X1.

Therefore, we suggest further studies on Kharita Formation at the southwest direction of well-X7.

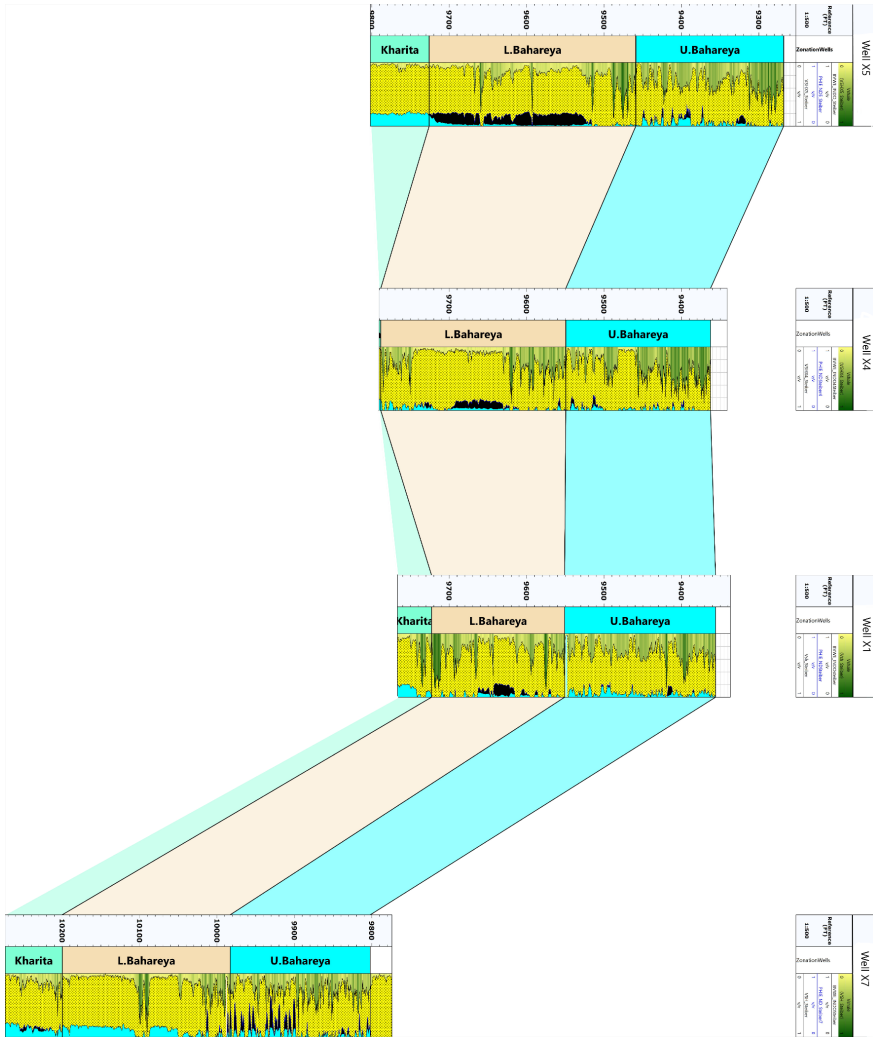


Fig. 15. Full correlation of all Shahd Field wells (X1, X4, X5 & X7).

**Acknowledgements.** The authors would like to thank the geophysics department of Cairo University for giving the permission to use all the available and needed software for the research. The authors would also like to thank the editors and reviewers of Contribution to Geophysics and Geodesy (CGG) for their guidance and constructive comments.

## References

- Abu El-Ata A. S. A., 1990: The role of seismic-tectonics in establishing the structural foundation and saturation conditions of El-Ginidi basin, western Desert, Egypt. In: Egyptian Geophysical Society (EGS), Proc. of the 8th Ann. Meeting, **14**, 150–189.
- Abuzaied M., Mabrouk W. M., Metwally A., Bakr A., Eldin S. E. S., 2020: Correlation of the reservoir characteristics from the well-logging data and core measurements in QASR field, north Western Desert, Egypt. Arab. J. Geosci., **13**, 3, 118, doi: 10.1007/s12517-020-5120-7.
- Alberty M. W., 1994: Standard interpretation; part 4—wireline methods. In: Morton-Thompson D., Woods A. M. (Eds.): Development Geology Reference Manual: AAPG Methods in Exploration Series 10, 180–185, consulted the 24/7/2021 in [https://wiki.aapg.org/Density-neutron\\_log\\_porosity](https://wiki.aapg.org/Density-neutron_log_porosity).
- Archie G. E., 1942: The electrical resistivity log as an aid in determining some reservoir characteristics. Pet. Trans. AIME, **146**, 1, 54–62, doi: 10.2118/942054-G.
- Bassiouni Z., 2012: Well Logs Quality Control Issues. Online, available at: <http://oilproduction.net/files/Well%20Logs%20Quality%20Control%20Issues.pdf>.
- Clavier C., Hoyle W. R., Meunier D., 1971: Quantitative Interpretation of Thermal Neutron Decay Time Logs: Part I. Fundamentals and Techniques. J. Pet. Tech., **23**, 6, 743–755, doi: 10.2118/2658-A-PA.
- De Witte L., 1950: Relation between resistivities and fluid contents of porous rocks. Oil Gas J., **49**, 16, 120–132.
- Hassan A. M., Mabrouk W. M., Farhoud K. M., 2014: Petrophysical analysis for Ammonite-1 well, Farafra Area, Western Desert, Egypt. Arab. J. Geosci., **7**, 12, 5107–5125, doi: 10.1007/s12517-013-1123-y.
- Kamel M. H., 1993: On water saturation determination. Egypt. Geol. Surv. Min. Author., **20**, 691–708.
- Kamel M. H., Helmi A., Bayoumi A. I., 1996: A new theoretical technique for evaluating reservoir parameters in shaly-sand section: application in an area in the Northern Gulf of Suez of Egypt: a case history. The 2nd Well Logging Symposium of Japan, September 26–27, 1996, Paper A.
- Kamel M. H., Mabrouk W. M., 2003: Estimation of shale volume using a combination of the three porosity logs. J. Pet. Sci. Eng., **40**, 3-4, 145–157, doi: 10.1016/S0920-4105(03)00120-7.
- Kassab M. A., Abdou A. A., El Gendy N. H., Shehata M. G., Abuhagaza A. A., 2017: Reservoir characteristics of some Cretaceous sandstones, North Western Desert, Egypt. Egypt. J. Pet., **26**, 2, 391–403, doi: 10.1016/j.ejpe.2016.05.011.
- Moretti I., Kerdraon Y., Rodrigo G., Huerta F., Griso J. J., Sami M., Said M., Ali H., 2010: South Alamein petroleum system (Western Desert, Egypt). Pet. Geosci., **16**, 2, 121–132, doi: 10.1144/1354-079309-004.
- Mostafa M. M., Fahmy M. M., Darwish M., Selim S. S., 2018: Geological 3D static model of Bahariya Formation. (Upper Albian-Cenomanian) Shahd/Shahd SE fields, Northern Western Desert, Egypt. Egypt. J. Geol., **62**, 1, 35–51, doi: 10.21608/EGJG.2018.216373.

- Pickett G. R., 1973: Pattern recognition as a means of formation evaluation. *Log Anal.*, **14**, 4, 3–11, consulted in [https://wiki.seg.org/wiki/Pickett\\_plot](https://wiki.seg.org/wiki/Pickett_plot).
- Poupon A., Leveaux J., 1971: Evaluation of water saturation in shaly formations. The SPWLA 12th Annual Logging Symposium, Dallas, Texas, 2-5 May, SPWLA-1971-0.
- Poupon A., Loy M. E., Tixier M. P., 1954: A contribution to electric log interpretation in shaly sands. *J. Pet. Technol.*, **6**, 6, 27–34, doi: 10.2118/311-G.
- Shazly T. F., 2009: The Impact of Pickett's Plot for Developing the Petrophysical Model of Abu Roash Reservoir in Ras Qattara Area, Western Desert, Egypt. In: Conference Proceedings, 4th EAGE North African/Mediterranean Petroleum and Geosciences Conference and Exhibition Tunis 2009, Mar 2009, European Association of Geoscientists & Engineers, doi: 10.3997/2214-4609.20145789.
- Simandoux P., 1963: Mesures Dielectriques en Milieu Poreux, Application à Mesure des saturations en Eau, Etude du Comportement des Massifs Argileux. *Revue de l'Institut Francais du Petrol*, Supplementary Issue.
- Soliman K., 2021: Optimizing models for lower Bahariya reservoir properties in Shahd SE field, East Ras Qattara concession, western desert, Egypt. Master thesis, Cairo university, 25–43.
- Steiber R. G., 1973: Optimization of shale volumes in open hole logs. *J. Pet. Technol.*, **31**, 147–162.
- Temraz M. G. M., Abdou A. A., Shehata M. G., 2009: Sedimentology of the Bahariya Formation in Salam-IX Well, Northern Western Desert, Egypt. *Petroleum Science and Technology*, **27**, 14, doi: 10.1080/10916460802608222.